Estimation of Secondary Organic Aerosol Viscosity from Explicit Modeling of Gas-Phase Oxidation of Isoprene and α-pinene

Tommaso Galeazzo[1], Richard Valorso[2], Ying Li[1], Marie Camredon[2], Bernard Aumont[2], and Manabu Shiraiwa[1]

[1]Department of Chemistry, University of California, Irvine, CA92625, USA
[2]LISA, CNRS/INSU UMR7583, Université Paris Est Créteil et Université Paris Diderot, Institut Pierre Simon Laplace, 94010 Créteil, France

Correspondence: M. Shiraiwa (m.shiraiwa@uci.edu)

Abstract. Secondary organic aerosols (SOA) are major components of atmospheric fine particulate matter, affecting climate and air quality. Mounting evidence exists that SOA can adopt glassy and viscous semisolid states, impacting formation and partitioning of SOA. In this study, we conduct explicit modeling of isoprene photooxidation and α-pinene ozonolysis and subsequent SOA formation using the GECKO-A (Generator of Explicit Chemistry and Kinetics of Organics in the Atmosphere) model. Our recently-developed parameterizations to predict glass transition temperature of organic compounds are implemented into a box model with explicit gas-phase chemical mechanisms to simulate viscosity of SOA. The effects of chemical composition, relative humidity, mass loadings and mass accommodation on particle viscosity are investigated in comparison with measurements of SOA viscosity. The simulated viscosity of isoprene SOA agrees well with viscosity measurements as a function of relative humidity, while the model underestimates viscosity of α-pinene SOA by a few orders of magnitude. This difference may be due to missing processes in the model including gas-phase dimerization and particle-phase reactions leading to the formation of high molar mass compounds that would increase particle viscosity. Additional simulations imply that kinetic limitations of bulk diffusion and reduction in mass accommodation coefficient may also play a role in enhancing particle viscosity by suppressing condensation of semi-volatile compounds. The developed model is a useful tool for analysis and investigation of the interplay among gas-phase reactions, particle chemical composition and SOA phase state.

1 Introduction

Secondary organic aerosols (SOA) are ubiquitous in the atmosphere and represent a major component of fine particulate matter, affecting air quality, climate and public health (Jimenez et al., 2009; Pöschl and Shiraiwa, 2015). Due to their complexity, SOA represent a large source of uncertainty in current understanding of global climate change and air pollution (Tsigaridis et al., 2014; Ciarelli et al., 2019). Development of SOA models represents one of the most challenging and demanding problems in atmospheric chemistry (Shrivastava et al., 2017). Formation of SOA is initiated by gas-phase oxidation of biogenic and anthropogenic volatile organic compounds (VOC) (Kroll and Seinfeld, 2008). Typically, multigenerational oxidation of VOC in the gas phase leads to the formation of a myriad of semi-volatile and low volatility compounds which can condense on pre-existing particles (Ziemann and Atkinson, 2012; Nozière et al., 2015) or contribute to nucleation and new particle formation

(Tröstl et al., 2016). As gas-phase oxidation is often regarded as the rate-limiting step of SOA formation, there is a strong
need for a computational tool enabling to generate exhaustive gas-phase chemical mechanisms. The GECKO-A (Generator
of Explicit Chemistry and Kinetics of Organics in the Atmosphere) model is to-date the most extensive generator of gas-
phase chemical schemes; based on established reaction pathways and structure-activity relationships, it automatically generates
detailed gas-phase mechanisms involving thousands-to-millions of oxidation products from a given VOC precursor (Aumont
et al., 2005, 2012; Lee-Taylor et al., 2011).

Most aerosol models treat SOA particles as homogeneous and well-mixed liquids with a dynamic viscosity (η) below 10^2
Pa s. Recent studies provide accumulating evidence that SOA can adopt glassy solid ($\eta \geq 10^{12}$ Pa s) or amorphous semi-
solid phase states ($10^2 \leq \eta < 10^{12}$ Pa s) depending on chemical composition, relative humidity (RH), and temperature (Koop
et al., 2011; Virtanen et al., 2010; Reid et al., 2018). The particle phase state is impacted by SOA chemical composition,
hygroscopicity and water content. Notably, water can act as a plasticizer lowering SOA viscosity (Mikhailov et al., 2009).
It has been observed that ambient SOA particles can bounce off from an impactor stage depending on ambient conditions,
indicating non-liquid states of organic particles (Virtanen et al., 2011; Bateman et al., 2017; Slade et al., 2019). Measurements
of the viscosity of SOA bulk materials derived from the oxidation of limonene (Hinks et al., 2016), toluene (Song et al., 2016),
α-pinene (Renbaum-Wolff et al., 2013; Kidd et al., 2014; Bateman et al., 2015; Zhang et al., 2015; Grayson et al., 2016;
Hosny et al., 2016) and isoprene (Song et al., 2015) have confirmed that viscosity of SOA particles can vary depending on
temperature and RH (Petters et al., 2019). In addition, previous studies have shown that SOA chemical composition can be
affected by experimental conditions upon SOA formation such as RH and particle mass concentrations (Kidd et al., 2014;
Hinks et al., 2016; Grayson et al., 2016; Jain et al., 2018). These results imply that SOA viscosity and phase state are dynamic
properties in response to chemical processing of organic aerosols and variations in RH and temperature in the atmosphere.

In liquid particles, molecules diffuse fast in the particle bulk, leading to rapid establishment of gas-particle equilibrium. In
glassy and viscous particles, kinetic limitations of bulk diffusion can significantly retard gas-particle partitioning, prolonging
equilibration timescales (Li and Shiraiwa, 2019; Mai et al., 2015; Vaden et al., 2011), while relatively fast particle-particle
mixing were observed at intermediate and high RH (Ye et al., 2016, 2018). Model simulations suggest that an assumption of
instantaneous equilibrium partitioning can result in substantial overestimation of particle mass concentration and underesti-
mation of gas-phase mass concentration (Shiraiwa et al., 2012). A proper consideration of particle phase state is essential for
simulating particle size distribution dynamics in SOA growth (Shiraiwa et al., 2013; Zaveri et al., 2018, 2020). Heterogeneous
and multiphase reactions (Kuwata and Martin, 2012; Shiraiwa et al., 2011; Davies and Wilson, 2015; Zhang et al., 2018; Mar-
shall et al., 2018; Zhou et al., 2019) as well as activation to cloud droplets and ice crystals (Slade et al., 2017; Knopf et al.,
2018) can also be impacted by glassy and amorphous semisolid states. Thus, it is important to consider the effects of particle
phase state on SOA processes for accurate representation of the fate of SOA particles in aerosol models.

Recently, we have developed parameterizations to predict glass transition temperature (T_g) of organic compounds based on
molar mass and atomic O:C ratio (Shiraiwa et al., 2017), elemental composition (i.e., number of carbon, hydrogen, oxygen,
nitrogen, and sulfur) (DeRieux et al., 2018), and volatility (Li et al., 2020). T_g is a characteristic temperature at which a phase
transition from a glassy solid state to an amorphous semi-solid state occurs (Koop et al., 2011). Applying the Gordon-Taylor

mixing rule for mixtures of SOA multiple components and water, the viscosity of SOA can be estimated by the T_g-scaled
Arrhenius plot of viscosity (DeRieux et al., 2018). This method has been successfully applied to estimate particle viscosity
based on elemental composition obtained from high resolution mass spectrometry (Schum et al., 2018; Ditto et al., 2019; Song
et al., 2019).

In this study, the T_g and viscosity prediction methods are implemented into the GECKO-A and box model. Model simu-
lations with explicit chemical mechanisms are conducted to reproduce chamber experimental conditions for SOA generation
and subsequent viscosity measurements. The effects of chemical composition and mass accommodation on SOA partitioning
and viscosity are also investigated. The objective of this work is to expand our understanding on the relationship and interplay
among gas-phase reactions, chemical composition and viscosity of SOA.

2 Methods

2.1 GECKO-A

GECKO-A generates detailed gas-phase chemical oxidation schemes and the associated gas-particle mass transfers for SOA
formation. It produces explicit highly detailed chemical mechanisms starting from experimental data and structure-activity
relationships (SARs) (Aumont et al., 2005). Implemented into a box model, these explicit chemical mechanisms simulate the
oxidation of parent VOC precursors to oxidation products, their subsequent gas-phase chemistry, as well as partitioning into
the particle phase based on their vapor pressures. The chemical mechanism does not account for gas-phase chemistry of species
with vapor pressure below 10^{-13} atm, which are assumed to be of enough low volatility to partition to the condensed phase. In
our simulations, species vapor pressures are estimated via the approach by Nannoolal et al. (Nannoolal et al., 2008).

The mechanism generator follows a reduction protocol optimizing the number of generated reactions and chemical species
(Valorso et al., 2011). This protocol has been established to reduce the computational cost of box-model simulations. In the gas
phase, isomer substitution is not allowed for position isomers when the overall yield for the product is > 5 %; otherwise only
the highest-yield positional isomer is considered. For each reaction, pathways with branching ratios < 5 % are not accounted
for and the main reaction branches are scaled proportionally (Valorso et al., 2011). The chemical mechanism accounts for
chemistry of peroxy and alkoxy radicals generated during precursors oxidation. SOA chemistry is a multi-generational process
and in our simulations the generated chemical schemes follow the chemistry of reaction products up to the 5th generation.
The GECKO-A version used in this study has been recently enriched with SARs estimations of alkoxy radical decomposition
and H-migration reaction rates (Vereecken and Peeters, 2009; La et al., 2016). Rate coefficients and branching ratios for gas-
phase reactions of OH with aliphatic compounds and peroxy radicals are estimated based on recent SAR investigations (Jenkin
et al., 2018a,b). Our simulations do not include autooxidation and condensed-phase chemistry, which represent limitations of
GECKO-A modeling.

α-pinene and isoprene oxidation mechanisms have been investigated extensively both in model and experimental studies.
Their oxidation mechanisms are well known, providing good estimations of resulting SOA composition. The SARs for both
α-pinene and isoprene oxidation are implemented into GECKO-A with state-of-the-art protocols estimating radical reactions

and respective rate constants. The base mechanism for α-pinene photooxidation and ozonolysis include a detailed description of reactions with OH radicals (McVay et al., 2016), and branch reactions identified via quantum and theoretical chemical calculations (Peeters et al., 2001; Vereecken et al., 2007). Stabilized Criegee intermediates (SCIs) chemistry is not treated

95 explicitly and stable products are directly assigned via a rule-base method. This scheme accounts for a direct reaction route to account for pinonaldehyde formation during the reaction of SCIs with water (McVay et al., 2016). The GECKO-A isoprene oxidation scheme follows the main protocol developed by Aumont et al. (Aumont et al., 2005) and branching reactions for isoprene + OH are also considered (Paulot et al., 2009). The chemical schemes for α-pinene and isoprene oxidation are composed of 84,000 and 1,900 species, and of $\sim$700,000 and $\sim$17,000 reactions, respectively.

100 ## 2.2 Box model and simulations setup

Each chemical mechanism is coupled to a box model representing SOA formation from α-pinene or isoprene oxidation in specific chamber experiments. The time evolution of species concentration is computed through a two-step method that explicitly solves stiff ordinary differential equations (Verwer, 1994; Verwer et al., 1996). The experimental conditions are summarized in Table 1. All laboratory experiments were performed in absence of seed particles, but the box model used in our simulations

105 does not treat nucleation. Thus, in our simulations the first steps of nucleation are approximated by the addition of seed particles with a particle radius of 5 nm and a concentration of 10^4 particles cm^{-3} (McVay et al., 2016). It is assumed that the density of SOA particles is 1.2 g cm^{-3} (Kuwata and Martin, 2012). The particle number concentration is also assumed to remain constant during simulations, while the particle radius evolves following the partitioning of organics. All simulations are conducted with a NOx mixing ratio of 3 ppt to reflect low NOx conditions of chamber and flow tube experiments. For all simulations we

110 consider reversible gas-wall partitioning of organic species with the vapor wall loss rate of 10^{-3} s^{-1} based on experimental observations (Lim and Ziemann, 2009; McVay et al., 2016). Photolysis rates are computed using the cross-sections and the quantum yields from Aumont et al. (Aumont et al., 2005). Photolysis conditions are set to average daylight conditions of a mid-latitude spring day for isoprene photooxidation simulations and to zero for α-pinene dark ozonolysis experiments, coherent with the experimental conditions.

115 For continuous flow reactor experiments, the concentrations of VOC precursors and oxidants were stable by continuous inflow and outflow of gases from the tube reactor; in the box model simulations precursor concentrations are fixed at steady state values as measured in corresponding experiments. In chamber batch experiments, the reactants were injected once at the beginning of the experiment and the concentrations evolved; in box model simulations the VOC precursor and ozone concentrations are initially set to the respective experimental values and species concentrations evolve due to gas oxidation,

120 gas-particle partitioning, and wall deposition. SOA particles were formed under dry conditions and then SOA were exposed to water vapor at different RH for viscosity measurements. For each set of simulations, the measured RH and temperature were used to constrain the simulation conditions. Note that partitioning of water is not considered in the box model as particle water uptake should be very minor under the very low RH values at which SOA particles were formed.

The box model treats the mass transfer of gaseous organic species to particles and to chamber walls. Gas-particle partitioning

125 is assumed to follow Raoult's law at equilibrium (La et al., 2016) (i.e., depending on the saturation vapor pressure of the

Table 1. Experimental conditions simulated in the box model to explore α-pinene and isoprene SOA viscosity, and simulated glass transition temperatures of dry SOA ($T_{\mathrm{g,org}}$).

Study	O_3 (ppb)	α-pinene (ppb)	RH	t (min.)	T (K)	Exp. setup*	$T_{\mathrm{g,org}}$ (K)
Renbaum-Wolff et al., 2013	300	100	0.5	30	298	Continuous flow PF-BM	275
Zhang et al., 2015	30000	700	0.5	6	293	Batch exp., DMA	258
Zhang et al., 2015	30000	700	0.5	1.5	293	Batch exp., DMA	263
Kidd et al., 2014	650	800	dry	30	297	Batch exp., PI	266
Grayson et al., 2016	68	100	0.5	80	298	Continuous flow, PF-BM	284
Bateman et al., 2014	100	300	0.5	174	298	Continuous flow, R	275
Study	O_3 (ppm)	isoprene (ppm)	RH	t (min.)	T (K)	Exp. setup*	$T_{\mathrm{g,org}}$ (K)
Song et al., 2015	10	4	13.0	1.4	293	Continuous flow, PF-BM	260

* Poke Flow Bead Mobility (PF-BM), Differential Mobility Analyzer (DMA), Particle Impactor (PI) + SEM, Rebound impactor (R).

organic compounds assuming ideal mixing). Gas to particle partitioning is described in the box model using the gas-particle mass transfer coefficient of a compound (k_{gp}, in s^{-1}) with the Fuchs-Sutugin approach in the transition regime as (Seinfeld and Pandis, 2016):

$$k_{\mathrm{gp}} = 4\pi D_{\mathrm{g}} r_{\mathrm{p}} N_{\mathrm{p}} \beta \tag{1}$$

130
$$\beta = \frac{0.75\alpha(1+K_{\mathrm{n}})}{K_{\mathrm{n}}^2 + K_{\mathrm{n}} + 0.283 K_{\mathrm{n}}\alpha + 0.75\alpha} \tag{2}$$

where D_{g} ($\mathrm{cm^2\,s^{-1}}$) is the gas diffusivity, r_{p} (cm) is the particle radius, N_{p} ($\mathrm{cm^{-3}}$) is the particle number concentration, K_{n} is the Knudsen number, and α is the mass accommodation coefficient. α, also termed as the bulk accommodation coefficient, represents the probability for a gas molecule colliding with surface to enter the bulk of the particle. Based on recent experiments and molecular dynamics simulations α is assumed to be unity for the base case scenario of our simulations (Liu et al., 2019;

135 Julin et al., 2014). This approach does not account for potential kinetic limitations caused by bulk diffusion in viscous particles.

A recent study has introduced an effective mass accommodation coefficient α_{eff}, which effectively considers the kinetics of accommodation at the surface, transfer across the gas-particle interface, and further transport into the particle bulk (Shiraiwa and Pöschl, 2021):

$$\alpha_{\mathrm{eff}} = \alpha_{\mathrm{s}} \frac{1}{1 + \dfrac{\alpha_{\mathrm{s}}\omega C_0}{4 D_{\mathrm{b}}\rho_{\mathrm{p}}} \cdot \dfrac{r_{\mathrm{p}}}{5} 10^{-12} \dfrac{\mathrm{g \cdot cm^{-3}}}{\mathrm{\mu g \cdot m^{-3}}}} \tag{3}$$

140   where α_s is the surface accommodation coefficient (i.e., the probability for a gas molecule colliding with surface to adsorb on the particle surface), ω (cm s^{-1}) is the mean thermal velocity of the organic compound in the gas phase, D_b (cm^2 s^{-1}) is diffusivity in the condensed phase, ρ_p (g cm^{-3}) is the particle density, and C_0 (μg m^{-3}) is the pure compound saturation mass concentration. Application of α_eff in the Fuchs-Sutugin approach (e.g., $\alpha = \alpha_\mathrm{eff}$) yields SOA partitioning with effective consideration of kinetic limitations induced by slow bulk diffusion in viscous particles. This approach can yield consistent

145   results with a detailed kinetic multilayer model (KM-GAP, Shiraiwa et al., 2012) and two-film model solutions (Zaveri et al., 2014). We implement this method to explore the effects of mass accommodation and kinetic partitioning on predicted viscosity by comparing with the base case scenario (e.g., α fixed to 1).

2.3   Viscosity prediction implementation

The glass transition temperature of an organic compound i ($T_{\mathrm{g},i}$) can be estimated with the following recently-developed

150   parameterization based on its elemental composition (DeRieux et al., 2018).

$$T_{\mathrm{g},i} = (n_\mathrm{C}^0 + \ln(n_\mathrm{C}))b_\mathrm{C} + b_\mathrm{H} \cdot \ln(n_H) + b_\mathrm{CH} \cdot \ln(n_\mathrm{C}) \cdot \ln(n_H) + b_\mathrm{O} \cdot \ln(n_\mathrm{O}) + b_\mathrm{CO} \cdot \ln(n_\mathrm{C}) \cdot \ln(n_\mathrm{O}) \tag{4}$$

Where the coefficient values for [n_C^0, b_C, b_H, b_CH, b_O, and b_CO] are [1.96, 61.99, -113.33, 28.74, 0, 0] for CH compounds and [12.13, 10.95, -41.82, 21.61, 118.96, -24.38] for CHO compounds. We have also included the recently developed parametrization for CHON compounds by Li et al. (Li et al., 2020):

155   $$T_{\mathrm{g},i} = (n_\mathrm{C}^0 + \ln(n_\mathrm{C}))b_\mathrm{C} + \ln(n_\mathrm{O})b_\mathrm{O} + \ln(n_\mathrm{N})b_\mathrm{N} + \ln(n_\mathrm{C})\ln(n_\mathrm{O})b_\mathrm{CO} + \ln(n_\mathrm{C})\ln(n_\mathrm{N})b_\mathrm{CN} + \ln(n_\mathrm{O})\ln(n_\mathrm{N})b_\mathrm{ON} \tag{5}$$

Where the coefficient values for [n_C^0, b_C, b_O, b_N, b_CO, b_CN, b_O] are [5.34, 31.53, -7.06, 134.96, 6.54, -34.36, and -15.35]. These parametrizations can predict $T_{\mathrm{g},i}$ with an uncertainty of about ±30 K; note that, however, in multicomponent SOA mixtures this uncertainty would be much smaller for ideal mixing conditions (Shiraiwa et al., 2017; DeRieux et al., 2018; Li et al., 2020). The T_g of a mixture of organic compounds (e.g. dry SOA) can be estimated using the Gordon-Taylor equation

160   with a Gordon-Taylor constant (k_GT) of 1: $T_{\mathrm{g,org}} = \Sigma_i \omega_i T_{\mathrm{g},i}$, where ω_i is the mass fraction of compound i (Dette et al., 2014).

    The Gordon-Taylor equation can also be used to estimate the glass transition temperature of mixtures of organic compounds and water ($T_\mathrm{g}(w_\mathrm{org})$):

$$T_\mathrm{g}(w_\mathrm{org}) = \frac{(1 - w_\mathrm{org}) \cdot T_\mathrm{g,w} + \dfrac{1}{k_\mathrm{GT}} \cdot w_\mathrm{org} T_\mathrm{g,org}}{(1 - w_\mathrm{org}) + \dfrac{1}{k_\mathrm{GT}} \cdot w_\mathrm{org}} \tag{6}$$

where w_org is the mass fraction of organics, $T_\mathrm{g,w}$ is the glass transition temperature of pure water (136 K), and k_GT is the

165   Gordon-Taylor constant which is assumed to be 2.5 (Koop et al., 2011; Zobrist et al., 2008). The w_org is calculated using the

mass concentration of water (m_{H_2O}) and of the organics in SOA (m_{SOA}) as: $w_{org} = m_{SOA} / (m_{SOA} + m_{H_2O})$. m_{H_2O} can be calculated using the Kohler theory with effective hygroscopicity parameter (κ) (Petters and Kreidenweis, 2013).

Once $T_g(w_{org})$ has been computed, the viscosity (η) can be derived with the following equation based on the Vogel-Tammann-Fulcher approach (DeRieux et al., 2018):

$$\log(\eta) = -5 + 0.434 \cdot \frac{T_0 D}{T - T_0} \tag{7}$$

$$T_0 = \frac{39.17 \cdot T_g(w_{org})}{D + 39.17} \tag{8}$$

where T_0 is the Vogel temperature and D is the fragility parameter. The D value is assumed to be 10 based on previous studies (Shiraiwa et al., 2017; DeRieux et al., 2018).

Viscosity can then be converted into bulk diffusivity using the Stokes-Einstein equation:

$$D_b = \frac{kT}{6\pi a \eta} \tag{9}$$

where k is the Boltzmann constant (1.38×10^{-23} J K^{-1}), T is the temperature (K), and a is the effective molecular radius (m). This relation, however, may not be accurate for very high viscosities and needs to be corrected with the fractional Stokes-Einstein (FSE) relation (Evoy et al., 2019):

$$D_b = D_{b,c} \cdot \left(\frac{\eta_c}{\eta}\right)^\xi \tag{10}$$

where ξ is an empirical fit parameter with the value of 0.93 (Evoy et al., 2019), η_c is the crossover viscosity with the value of 10^{-3} Pa s, and $D_{b,c}$ is the crossover diffusion coefficient at $\eta_c = 10^{-3}$ Pa s as determined by the Stokes-Einstein equation (9).

3 Results

3.1 Viscosity predictions of isoprene and α-pinene SOA

Figure 1 shows the measured and simulated viscosities of isoprene SOA, showing a very good agreement with experimental observations. SOA generated by isoprene ozonolysis adopt a semi-solid state for RH < 40 % and a liquid state for RH > 60 %. The model predicted $T_{g,org}$ is 260 K, which is in agreement with a previous estimation of 255 K (Berkemeier et al., 2014). All simulated viscosities with κ = 0.1 fall within uncertainties of experimental measurements except at 70 % RH, which is slightly below the lower bound of the error bar of experimental measurements. The simulated O:C ratio is 1.0, which is within
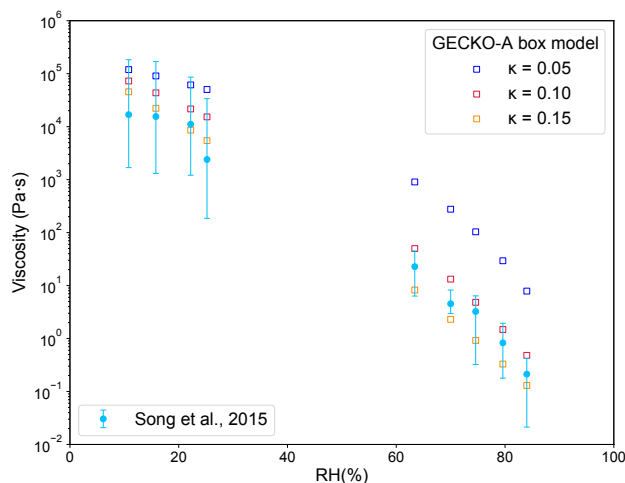
Figure 1. Viscosity of isoprene SOA as a function of RH. Circle markers with error bars represent measurements and associated uncertainties by Song et al. (Song et al., 2015) and square markers represent simulations with the GECKO-A box-model with different κ values.

190 the range of their estimation of 0.64 - 1.1 based on previous chamber experiments (Song et al., 2015). To examine the effects of κ on the calculated viscosity of isoprene SOA, sensitivity studies are conducted by varying κ within the range of 0.05–0.15, showing that lower and higher κ would lead to higher and lower viscosity, respectively.

Isoprene photooxidation in chamber experiments was conducted with very high precursor concentrations and a short reaction time such that a traditional gas-phase oxidation scheme dominates, which can be captured well in GECKO-A (Aumont

195 et al., 2005). Note that the formation of isoprene epoxydiols (IEPOX) (Paulot et al., 2009; Bates et al., 2014) and subsequent uptake of IEPOX into acidic particles followed by a series of multiphase reactions including the formation of oligomers and organosulfates (Riva et al., 2019) are found to be important in the ambient atmosphere (Wennberg et al., 2018). The uptake of IEPOX can be limited by bulk diffusion in a viscous matrix (Zhang et al., 2018) and IEPOX-SOA is reported to have high viscosity (Riva et al., 2019). For viscosity simulations of atmospherically relevant IEPOX-derived SOA, IEPOX multiphase

200 processes would need to be treated in future studies.

Figure 2 shows viscosity of α-pinene SOA measured in a number of studies and the corresponding simulated results by the GECKO-A box model for each experimental condition. Based on previous laboratory measurements κ was assumed to be 0.1 (Lambe et al., 2011; Pajunoja et al., 2014; Petters et al., 2019). Overall, the model simulations can reproduce the RH-dependent viscosity of α-pinene SOA, showing that α-pinene SOA is semi-solid between 0-65 % RH and liquid for RH > 65 % at the room

205 temperature. Simulated viscosity values of α-pinene SOA are by a few orders of magnitude higher than the ones simulated for isoprene SOA, which is consistent with experimental observations. Simulation results for Renbaum-Wolff's and Grayson's experiments fall within uncertainties of experimental measurements for the 40-60 % RH range. In simulations for Renbaum-Wolff's experiments at RH > 60 %, the predicted viscosity values are about one order of magnitude lower than the measured values. Larger deviations are observed for RH < 40 %, where simulated viscosities are up to four orders of magnitude lower than
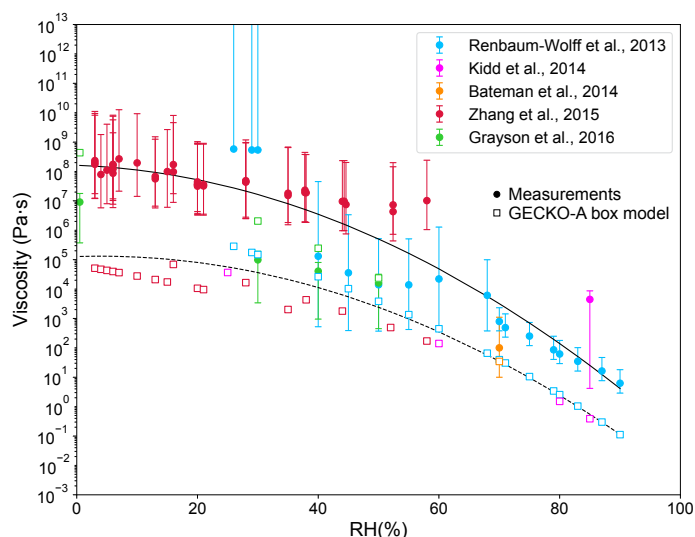
Figure 2. Comparison of measured (solid markers) and simulated (open markers) viscosity of α-pinene SOA as a function of RH. For each set of laboratory experiments the measured viscosities are reported with uncertainties. The solid and dashed lines represent the polynomial regression for measurements and model simulations, respectively, to guide eyes.

experimental measurements. The simulated viscosities are about one order of magnitude higher than Graysons's measurements for 20 < RH < 40 %. The simulated viscosity for Bateman's experiment agrees well with the observed experimental value within uncertainties. Kidd et al. (Kidd et al., 2014) provided only one data point at 85 % RH, which also represents inferred viscosity based on their impactor measurement; the predicted viscosity is three orders of magnitude below the inferred value, but only one order of magnitude below its lower bound. For simulations of Zhang et al. (Zhang et al., 2015), our predictions are about three to four orders of magnitude lower than measurements.

The simulated $T_{g,org}$ are within 255-285 K (see Table 1), which is in good agreement with a previous estimation of 278 K (Berkemeier et al., 2014) and a measurement of 272 K (Petters et al., 2019). To assess overall performance of our viscosity predictions, measured and simulated viscosities were fitted respectively with a second-order polynomial regression. While the RH dependence of viscosity is very well captured by our simulations, the simulated values underestimate viscosity by about two or three orders of magnitude on average. The variance of model simulations and experimental measurements is very similar ($R^2 = 0.85$), indicating that the GECKO-A box model can reproduce the variability observed in experimental measurements with different experimental conditions.

Grayson et al. (Grayson et al., 2016) investigated the impact of SOA mass loadings on viscosity, observing lower viscosity with higher SOA mass concentrations in the range of $10^2 - 10^4$ µg m^{-3}. We conducted four different simulations where precursor concentrations were varied in the range of the experimental values to match the final SOA mass loadings. As shown in Fig. 3, our simulated viscosities are within the experimental uncertainties, capturing this dependence very well. At higher mass loadings, compounds with relatively high volatility and low T_g can condense on particles, leading to a reduction of SOA
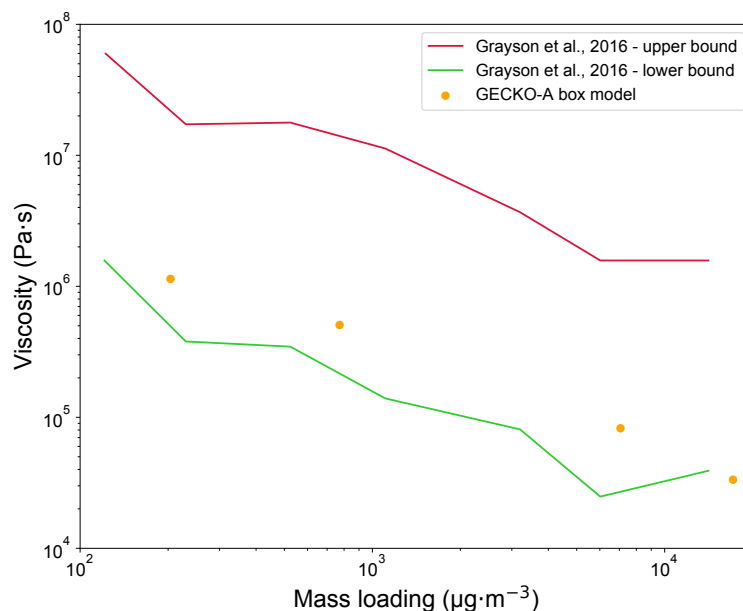
Figure 3. Impacts of SOA mass loadings on viscosity of α-pinene SOA. The red and green lines represent the upper and lower bounds of measured viscosity in Grayson et al., 2016. Orange markers represent simulated viscosities by the GECKO-A box model.

viscosity; for lower mass loadings, condensation of lower volatility compounds with higher T_g would be dominant, resulting in higher viscosity.

3.2 Chemical composition and functional group distributions of SOA

The GECKO-A box model tracks the concentrations of species both in the gas and particle phases, while retaining information on molecular properties including molar mass, O:C ratio, vapor pressure, and volatility or pure compound saturation mass concentration (C_0). Figure 4 shows most abundant particle-phase 500 compounds in simulated isoprene and α-pinene SOA products in the 2-dimensional volatility basis set framework of O:C ratio vs. $\log C_0$ (Donahue et al., 2011). The markers are color-coded with T_g and the marker size is scaled with particle-phase concentration in each simulation. Compounds with lower volatility tend to have higher O:C ratio and higher T_g, in good agreement with recent experimental and model studies (Zhang et al., 2019; Li et al., 2020). Isoprene oxidation products are found to have higher O:C ratio, while α-pinene oxidation products have lower C_0 and higher T_g. Note that, dark ozonolysis experiments of α-pinene have been conducted with an OH scavenger, which may contribute to lower O:C ratios for α-pinene ozonolysis products in the absence of OH oxidation. These results are in line with higher viscosity of α-pinene SOA compared to isoprene SOA, as measured and modeled in Figs. 1 and 2.

Our method to estimate T_g of organic compounds and SOA viscosity are based on elemental composition without accounting for molecular structure and specific intramolecular interactions. Some organic compounds with reactive functional groups may undergo particle-phase reactions, which are not treated in our simulations. To explore these aspects, we investigate the
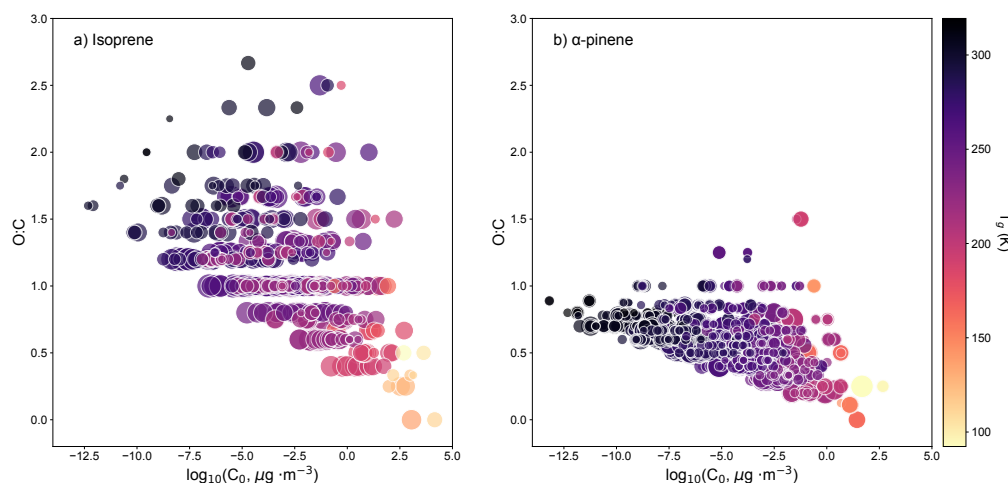
Figure 4. Chemical composition of SOA derived from oxidation of (a) isoprene and (b) α-pinene of all simulated experimental conditions reported in Table 1 plotted in the 2D-VBS framework of volatility and O:C ratio. Markers represent 500 most abundant particle-phase compounds from each simulation. The markers are color-coded with T_g. The marker size is scaled with particle phase concentration in each simulation.

functional groups distributions computed by GECKO-A and box modeling. The simulated functionality group distributions

245 of particle-phase SOA compounds are shown in Fig. 5. Most experiments led to similar chemical composition with high concentrations of ketones (–RC(O)R) and hydroperoxides (–ROOH), followed by slightly lower concentrations of aldehydes (–RCHO), alcohols (–ROH) and carboxylic acids (–RC(O)OH). The simulations for Grayson's experiments are characterized by the highest concentrations of –ROOH and –ROH, and by lower fractions of –RCHO. The simulations for Kidd's experiments show the second highest abundance of –ROH and noticeable amounts of –RC(O)OR. The simulation for Bateman's experiment

250 is characterized by high –RC(O)R abundance. A previous study suggested that the hydrogen-bond formation among organic compounds in the SOA organic matrix may influence the viscosity of α-pinene SOA significantly (Kidd et al., 2014). It has been further shown that alcohol and carboxylic acid groups can increase viscosity due to the formation of hydrogen bonding and ionic interactions if carboxylic acids are dissociated (Grayson et al., 2016; Rothfuss and Petters, 2017). These effects are not explicitly considered in our viscosity estimation method, which may be one of the reasons for the discrepancies between

255 measurements and simulations of SOA viscosity.

Chemical composition simulated for Zhang's experiments is characterized by the highest –RCHO fraction among all experiments, which may explain the largest difference between predicted and measured viscosities. Aldehydes are known to be highly reactive in the condensed phase by reacting with alcohols and hydroperoxides to form peroxyhemiacetals and oligomers (Ziemann and Atkinson, 2012) Such multiphase reactions could be accelerated under acidic conditions in the presence of car-

260 boxylic acids (Bakker-Arkema and Ziemann, 2020; Shiraiwa et al., 2013). In addition, the GECKO-A model treats neither
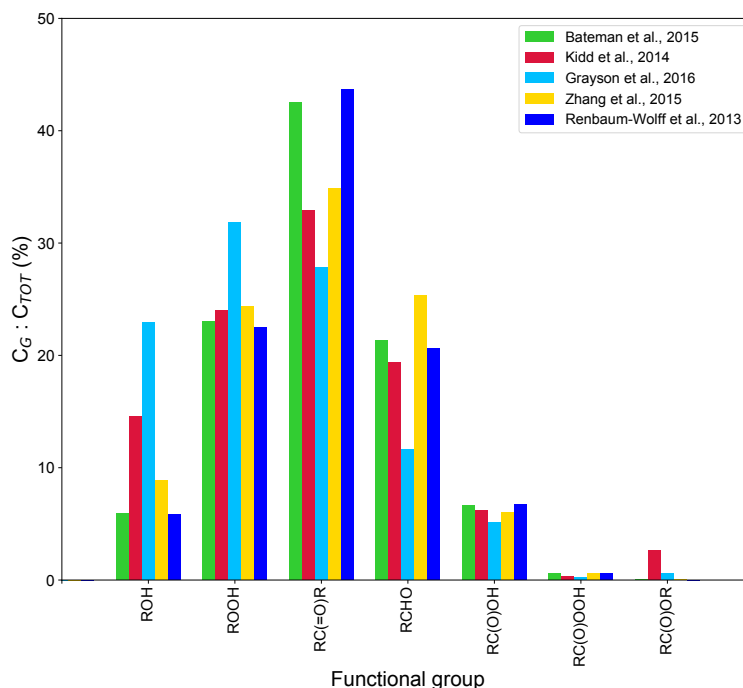
Figure 5. Simulated functional group distributions in particle-phase compounds derived from α-pinene ozonolysis for various experiments.

autoxidation to form highly oxygenated organic molecules (HOMs) nor gas-phase dimerization reactions of peroxy radicals, which are recently found to play a significant role in SOA formation and growth (Bianchi et al., 2019). These higher molar mass compounds with very low volatility have higher T_g, hence leading to higher SOA viscosity (Koop et al., 2011; Zhang et al., 2019; Champion et al., 2019; Li et al., 2020). While the extent of effects of these processes may vary among reaction con-
265 ditions applied in each experiment, the lack of treatment of these processes may be another plausible reason of lower simulated viscosity compared to experimental measurements.

3.3 Effects of mass accommodation

All the above simulations were conducted with mass accommodation coefficient equal to unity. Hereby, we investigate potential kinetic limitations of bulk diffusion on SOA partitioning and resulting viscosity by simulating two distinct experimental
270 conditions of flow tube experiments by Renbaum-Wolff et al. (Renbaum-Wolff et al., 2013) and batch experiments by Kidd et al. (Kidd et al., 2014). The effective mass accommodation coefficient (α_{eff}) is computed with Eq. 3, which is implemented into Eq. 1 and 2 to simulate partitioning that effectively accounts for kinetic limitations of bulk diffusion.

Figure 6 shows the simulated viscosity estimations for SOA formation under dry conditions followed by water exposure at different RH. Final viscosity values are higher for simulations with α_{eff} compared to those with α fixed to 1. For simulations of
275 Kidd's experiments, there is a large difference by several orders of magnitude in viscosity between two simulations of different
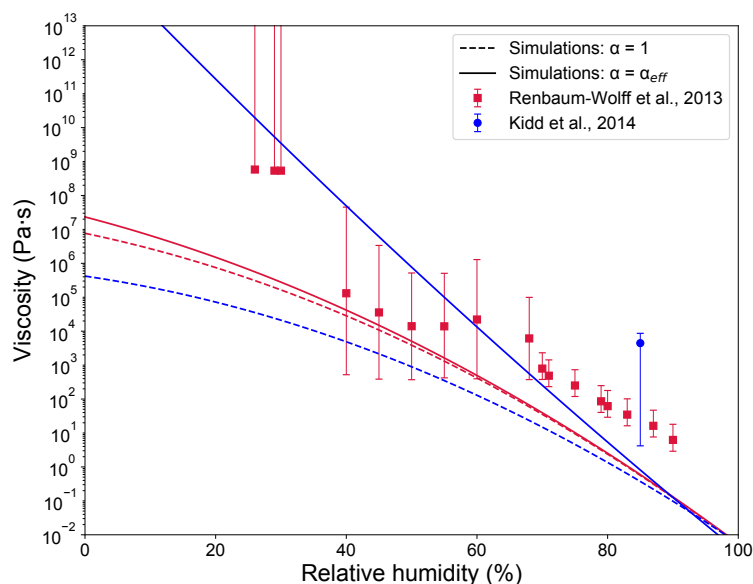
Figure 6. Simulated viscosities of α-pinene SOA with experimental conditions of Kidd et al. (2014) (blue) and Renbaum-Wolff et al. (2013) (red). The simulations were conducted in two different scenarios: $\alpha = 1$ (dashed lines) and $\alpha = \alpha_{\mathrm{eff}}$ (solid lines).

α when RH < 40 %; for example, at 40 % RH the simulated SOA viscosity is $\sim 10^4$ Pa s with $\alpha = 1$, while it is $\sim 10^8$ Pa s with $\alpha = \alpha_{\mathrm{eff}}$. This large difference stems from a stark reduction of α_{eff} for semivolatile compounds in a glassy solid matrix, which would prevent condensation of semi-volatile compounds with relatively low T_{g}; α_{eff} for low volatile compounds with higher T_{g} remains still close to unity allowing condensation, resulting in solidification of SOA particles.

280   This effect is reflected on the low simulated SOA mass loading of Kidd's experiments. When $\alpha = \alpha_{\mathrm{eff}}$ the simulated SOA mass loading is 15 µg m^{-3}, which is much lower than the simulation with $\alpha = 1$ (i.e. 7000 µg m^{-3}), where higher volatility compounds would condense without kinetic limitations, resulting in lower viscosity. The observed mass loadings during Kidd et al. (Kidd et al., 2014) chamber experiments were approximately ~ 1000 µg m^{-3}. This indicates that particle viscosity and resulting kinetic limitations may be overestimated in α_{eff} simulations or particle-phase reactions contribute substantially on

285   SOA formation, as discussed in Sect. 3.2. The predicted viscosities for the two scenarios for Renbaum-Wolff's experiments are very similar. In both scenarios, particles are liquid for RH > 65 % and semi-solid at RH < 65 %. The mass loadings simulated for Renbaum-Wolff's experiments are on the same order being 15 and 79 µg m^{-3} for simulations with α_{eff} and $\alpha = 1$, respectively. Both results are close with the experimental measurement value of ~ 50 µg m^{-3}. Kidd et al. (Kidd et al., 2014) applied higher oxidant and precursor concentrations (Table 1), resulting in larger effects of mass loadings and hence mass accommodation.

290   As viscosity measurements were not conducted at lower RH in Kidd et al. (Kidd et al., 2014) and time evolution of SOA mass concentrations and viscosity are unavailable for both studies, it is hard to fully resolve impacts of mass accommodation in this study; we intend to investigate this aspect in a follow-up study.

4 Conclusions

We applied the T_g parameterizations and viscosity prediction method in the GECKO-A box model to simulate the evolution
295 of viscosity and composition of SOA generated via α-pinene and isoprene oxidation. A range of simulations were performed
with experimental conditions applied for viscosity measurements in order to explore various effects such as chemical com-
position, relative humidity, mass loadings, and mass accommodation coefficient on SOA viscosity. Simulated viscosities are
consistent with the observed RH-dependence of viscosity for α-pinene and isoprene SOA, demonstrating the robustness of our
viscosity prediction method. Simulated viscosity values for isoprene SOA are in good agreement with measurements, while
300 those for α-pinene SOA were by a few orders of magnitude lower than experimental measurements. The simulated chemical
composition and functional group distributions indicate that α-pinene SOA contain substantial amounts of aldehydes, ketones,
and carboxylic acids. These compounds are reactive and may undergo dimerization and oligomerization reactions. In addition,
GECKO-A does not treat detailed chemistry involving stabilized Criegee intermediates, autoxidation and gas-phase dimeriza-
tion by peroxy radicals. These processes are known to lead to the formation of high molecular mass compounds that would
305 increase viscosity of SOA. Moreover, the model assumes that gas-particle partitioning of organics follows Raoult's law with
ideal mixing conditions. The implementation of these processes are warranted in future studies for better representation of
SOA chemical composition and viscosity.

Experiments were conducted to form SOA under dry conditions followed by water exposure for viscosity measurements
and it was unnecessary to consider uptake of water into the condensed phase upon SOA formation. Previous studies have
310 suggested that water vapor can significantly affect the composition of SOA. At higher RH water vapor interacts with Criegee
intermediates, leading to production of carboxylic acids or aldehydes and ketones via decomposition routes (Kristensen et al.,
2014). Kidd et al. (Kidd et al., 2014) have reported that as the RH at which the SOA is formed increases, there is a decrease
in viscosity, accompanied by an increasing contribution from carboxylic acids and a decreasing contribution from higher
molecular mass products. These aspects including chemistry of Criegee intermediates and water uptake should be a subject of
315 future studies for simulating particle viscosity under humid conditions.

We have also explored the effects of kinetic partitioning by accounting for reduction of mass accommodation coefficient
in a semisolid or viscous phase. The simulation results suggest that kinetic limitations in the particle phase would result in a
decrease in SOA mass loading and an increase in viscosity due to suppression of condensation of semi-volatile compounds. It
is still challenging to accurately assess the extent of this effect on viscosity due to the lack of experimental data for comparison
320 and to the absence of some chemical processes in our modeling method. Future experiments with simultaneous measurements
of chemical composition in the gas and particle phases as well as particle viscosity under different RH conditions will be
enormously helpful to further improve and constrain the model. While this study simulated viscosity of pure organic particles,
future studies should also investigate viscosity of inorganic-organic particles and effects of non-ideal interactions including
phase separation (Zuend and Seinfeld, 2012; You et al., 2014) and gel formation (Richards et al., 2020). The developed model
325 in this study is a useful tool for further exploration of phase state of atmospherically relevant SOA and it should also be useful
in refining the representation of SOA chemical evolution and phase state in regional and global air quality models.

Acknowledgements. MS acknowledges the Make Our Planet Great Again (MOPGA) short stay program by the Campus France, which enabled MS to have a one-month research stay at LISA hosted by BA in summer 2018. This work was also funded by the National Science Foundation (AGS-1654104) and the Department of Energy (DE-SC0018349).

330 *Author contributions.* TG, BA, and MS designed the study. TG and MS conducted simulations and data analysis. BA, RV, MC developed the GECKO-A and box models and provided a training on the tools. YL developed the T_g parameterizations. TG and MS wrote the manuscript with contributions from all coauthors.

Competing interests. The authors declare that they have no conflict of interest.

Data availability. The simulation data may be obtained from the corresponding author upon request.

References

Aumont, B., Szopa, S., and Madronich, S.: Modelling the evolution of organic carbon during its gas-phase tropospheric oxidation: development of an explicit model based on a self generating approach, Atmos. Chem. Phys., 5, 703–754, https://doi.org/10.5194/acpd-5-703-2005, 2005.

Aumont, B., Valorso, R., Mouchel-Vallon, C., Camredon, M., Lee-Taylor, J., and Madronich, S.: Modeling SOA formation from the oxidation of intermediate volatility n-alkanes, Atmos. Chem. Phys., 12, 7577–7589, https://doi.org/10.5194/acp-12-7577-2012, 2012.

Bakker-Arkema, J. G. and Ziemann, P. J.: Measurements of Kinetics and Equilibria for the Condensed Phase Reactions of Hydroperoxides with Carbonyls to Form Peroxyhemiacetals, ACS Earth Sp. Chem., 4, 467–475, https://doi.org/10.1021/acsearthspacechem.0c00008, 2020.

Bateman, A. P., Bertram, A. K., and Martin, S. T.: Hygroscopic influence on the semisolid-to-liquid transition of secondary organic materials, J. Phys. Chem. A, 119, 4386–4395, https://doi.org/10.1021/jp508521c, 2015.

Bateman, A. P., Gong, Z., Harder, T. H., De Sá, S. S., Wang, B., Castillo, P., China, S., Liu, Y., O'Brien, R. E., Palm, B. B., Shiu, H. W., Cirino, G. G., Thalman, R., Adachi, K., Lizabeth Alexander, M., Artaxo, P., Bertram, A. K., Buseck, P. R., Gilles, M. K., Jimenez, J. L., Laskin, A., Manzi, A. O., Sedlacek, A., Souza, R. A., Wang, J., Zaveri, R., and Martin, S. T.: Anthropogenic influences on the physical state of submicron particulate matter over a tropical forest, Atmos. Chem. Phys., 17, 1759–1773, https://doi.org/10.5194/acp-17-1759-2017, 2017.

Bates, K. H., Crounse, J. D., St. Clair, J. M., Bennett, N. B., Nguyen, T. B., Seinfeld, J. H., Stoltz, B. M., and Wennberg, P. O.: Gas phase production and loss of isoprene epoxydiols, J. Phys. Chem. A, 118, 1237–1246, https://doi.org/10.1021/jp4107958, 2014.

Berkemeier, T., Shiraiwa, M., Pöschl, U., and Koop, T.: Competition between water uptake and ice nucleation by glassy organic aerosol particles, Atmos. Chem. Phys., 14, 12 513–12 531, https://doi.org/10.5194/acp-14-12513-2014, 2014.

Bianchi, F., Kurtén, T., Riva, M., Mohr, C., Rissanen, M. P., Roldin, P., Berndt, T., Crounse, J. D., Wennberg, P. O., Mentel, T. F., Wildt, J., Junninen, H., Jokinen, T., Kulmala, M., Worsnop, D. R., Thornton, J. A., Donahue, N., Kjaergaard, H. G., and Ehn, M.: Highly Oxygenated Organic Molecules (HOM) from Gas-Phase Autoxidation Involving Peroxy Radicals: A Key Contributor to Atmospheric Aerosol, Chem. Rev., 119, 3472–3509, https://doi.org/10.1021/acs.chemrev.8b00395, 2019.

Champion, W. M., Rothfuss, N. E., Petters, M. D., and Grieshop, A. P.: Volatility and Viscosity Are Correlated in Terpene Secondary Organic Aerosol Formed in a Flow Reactor, Environ. Sci. Technol. Lett., 6, 513–519, https://doi.org/10.1021/acs.estlett.9b00412, 2019.

Ciarelli, G., Colette, A., Schucht, S., Beekmann, M., Andersson, C., Manders-Groot, A., Mircea, M., Tsyro, S., Fagerli, H., Ortiz, A. G., Adani, M., Briganti, G., Cappelletti, A., D'Isidoro, M., Cuvelier, C., Couvidat, F., Meleux, F., and Bessagnet, B.: Long-term health impact assessment of total PM2.5 in Europe during the 1990–2015 period, Atmos. Environ. X, 3, 100 032, https://doi.org/10.1016/j.aeaoa.2019.100032, 2019.

Davies, J. F. and Wilson, K. R.: Nanoscale interfacial gradients formed by the reactive uptake of OH radicals onto viscous aerosol surfaces, Chem. Sci., 6, 7020–7027, https://doi.org/10.1039/c5sc02326b, 2015.

DeRieux, W. S. W., Li, Y., Lin, P., Laskin, J., Laskin, A., Bertram, A. K., Nizkorodov, S. A., and Shiraiwa, M.: Predicting the glass transition temperature and viscosity of secondary organic material using molecular composition, Atmos. Chem. Phys., 18, 6331–6351, https://doi.org/10.5194/acp-18-6331-2018, 2018.

Dette, H. P., Qi, M., Schröder, D. C., Godt, A., and Koop, T.: Glass-forming properties of 3-methylbutane-1,2,3-tricarboxylic acid and its mixtures with water and pinonic acid, J. Phys. Chem. A, 118, 7024–7033, https://doi.org/10.1021/jp505910w, 2014.

Ditto, J. C., Joo, T., Khare, P., Sheu, R., Takeuchi, M., Chen, Y., Xu, W., Bui, A. A. T., Sun, Y., Ng, N. L., and Gentner, D. R.: Effects of Molecular-Level Compositional Variability in Organic Aerosol on Phase State and Thermodynamic Mixing Behavior, Environ. Sci. Technol., 53, 13 009–13 018, https://doi.org/10.1021/acs.est.9b02664, 2019.

375 Donahue, N. M., Epstein, S. A., Pandis, S. N., and Robinson, A. L.: A two-dimensional volatility basis set: 1. organic-aerosol mixing thermodynamics, Atmos. Chem. Phys., 11, 3303–3318, https://doi.org/10.5194/acp-11-3303-2011, 2011.

Evoy, E., Maclean, A. M., Rovelli, G., Li, Y., Tsimpidi, A. P., Karydis, V. A., Kamal, S., Lelieveld, J., Shiraiwa, M., Reid, J. P., and Bertram, A. K.: Predictions of diffusion rates of large organic molecules in secondary organic aerosols using the Stokes-Einstein and fractional Stokes-Einstein relations, Atmos. Chem. Phys., 19, 10 073–10 085, https://doi.org/10.5194/acp-19-10073-2019, 2019.

380 Grayson, J. W., Zhang, Y., Mutzel, A., Renbaum-Wolff, L., Böge, O., Kamal, S., Herrmann, H., Martin, S. T., and Bertram, A. K.: Effect of varying experimental conditions on the viscosity of α-pinene derived secondary organic material, Atmos. Chem. Phys., 16, 6027–6040, https://doi.org/10.5194/acp-16-6027-2016, 2016.

Hinks, M. L., Brady, M. V., Lignell, H., Song, M., Grayson, J. W., Bertram, A. K., Lin, P., Laskin, A., Laskin, J., and Nizkorodov, S. A.: Effect of viscosity on photodegradation rates in complex secondary organic aerosol materials, Phys. Chem. Chem. Phys., 18, 8785–8793,
385 https://doi.org/10.1039/c5cp05226b, 2016.

Hosny, N. A., Fitzgerald, C., Vyšniauskas, A., Athanasiadis, A., Berkemeier, T., Uygur, N., Pöschl, U., Shiraiwa, M., Kalberer, M., Pope, F. D., and Kuimova, M. K.: Direct imaging of changes in aerosol particle viscosity upon hydration and chemical aging, Chem. Sci., 7, 1357–1367, https://doi.org/10.1039/c5sc02959g, 2016.

Jain, S., Fischer, K. B., and Petrucci, G. A.: The influence of absolute mass loading of secondary organic aerosols on their phase state,
390 Atmosphere, 9, 131, https://doi.org/10.3390/atmos9040131, 2018.

Jenkin, M. E., Valorso, R., Aumont, B., Rickard, A. R., and Wallington, T. J.: Estimation of rate coefficients and branching ratios for gas-phase reactions of OH with aliphatic organic compounds for use in automated mechanism construction, Atmos. Chem. Phys., 18, 9297–9328, https://doi.org/10.5194/acp-18-9297-2018, 2018a.

Jenkin, M. E., Valorso, R., Aumont, B., Rickard, A. R., and Wallington, T. J.: Estimation of rate coefficients and branching ratios for gas-phase
395 reactions of OH with aromatic organic compounds for use in automated mechanism construction, Atmos. Chem. Phys., 18, 9329–9349, https://doi.org/10.5194/acp-18-9329-2018, 2018b.

Jimenez, J. L., Canagaratna, M. R., Donahue, N. M., Prevot, A. S., Zhang, Q., Kroll, J. H., DeCarlo, P. F., Allan, J. D., Coe, H., Ng, N. L., Aiken, A. C., Docherty, K. S., Ulbrich, I. M., Grieshop, A. P., Robinson, A. L., Duplissy, J., Smith, J. D., Wilson, K. R., Lanz, V. A., Hueglin, C., Sun, Y. L., Tian, J., Laaksonen, A., Raatikainen, T., Rautiainen, J., Vaattovaara, P., Ehn, M., Kulmala, M., Tomlinson,
400 J. M., Collins, D. R., Cubison, M. J., Dunlea, E. J., Huffman, J. A., Onasch, T. B., Alfarra, M. R., Williams, P. I., Bower, K., Kondo, Y., Schneider, J., Drewnick, F., Borrmann, S., Weimer, S., Demerjian, K., Salcedo, D., Cottrell, L., Griffin, R., Takami, A., Miyoshi, T., Hatakeyama, S., Shimono, A., Sun, J. Y., Zhang, Y. M., Dzepina, K., Kimmel, J. R., Sueper, D., Jayne, J. T., Herndon, S. C., Trimborn, A. M., Williams, L. R., Wood, E. C., Middlebrook, A. M., Kolb, C. E., Baltensperger, U., and Worsnop, D. R.: Evolution of organic aerosols in the atmosphere, Science (80-.)., 326, 1525–1529, https://doi.org/10.1126/science.1180353, 2009.

405 Julin, J., Winkler, P. M., Donahue, N. M., Wagner, P. E., and Riipinen, I.: Near-unity mass accommodation coefficient of organic molecules of varying structure, Environ. Sci. Technol., 48, 12 083–12 089, https://doi.org/10.1021/es501816h, 2014.

Kidd, C., Perraud, V., Wingen, L. M., and Finlayson-Pitts, B. J.: Integrating phase and composition of secondary organic aerosol from the ozonolysis of α-pinene, Proc. Natl. Acad. Sci. U. S. A., 111, 7552–7557, https://doi.org/10.1073/pnas.1322558111, 2014.

Knopf, D. A., Alpert, P. A., and Wang, B.: The Role of Organic Aerosol in Atmospheric Ice Nucleation: A Review, ACS Earth Sp. Chem.,
410   2, 168–202, https://doi.org/10.1021/acsearthspacechem.7b00120, 2018.

Koop, T., Bookhold, J., Shiraiwa, M., and Pöschl, U.: Glass transition and phase state of organic compounds: Dependency on molecular properties and implications for secondary organic aerosols in the atmosphere, Phys. Chem. Chem. Phys., 13, 19 238–19 255, https://doi.org/10.1039/c1cp22617g, 2011.

Kristensen, K., Cui, T., Zhang, H., Gold, A., Glasius, M., and Surratt, J. D.: Dimers in α-pinene secondary organic aerosol: Effect of hydroxyl
415   radical, ozone, relative humidity and aerosol acidity, Atmos. Chem. Phys., 14, 4201–4218, https://doi.org/10.5194/acp-14-4201-2014, 2014.

Kroll, J. H. and Seinfeld, J. H.: Chemistry of secondary organic aerosol: Formation and evolution of low-volatility organics in the atmosphere, Atmos. Environ., 42, 3593–3624, https://doi.org/10.1016/j.atmosenv.2008.01.003, 2008.

Kuwata, M. and Martin, S. T.: Phase of atmospheric secondary organic material affects its reactivity, Proc. Natl. Acad. Sci. U. S. A., 109,
420   17 354–17 359, https://doi.org/10.1073/pnas.1209071109, 2012.

La, Y. S., Camredon, M., Ziemann, P. J., Valorso, R., Matsunaga, A., Lannuque, V., Lee-Taylor, J., Hodzic, A., Madronich, S., and Aumont, B.: Impact of chamber wall loss of gaseous organic compounds on secondary organic aerosol formation: Explicit modeling of SOA formation from alkane and alkene oxidation, Atmos. Chem. Phys., 16, 1417–1431, https://doi.org/10.5194/acp-16-1417-2016, 2016.

Lambe, A. T., Onasch, T. B., Massoli, P., Croasdale, D. R., Wright, J. P., Ahern, A. T., Williams, L. R., Worsnop, D. R., Brune, W. H., and
425   Davidovits, P.: Laboratory studies of the chemical composition and cloud condensation nuclei (CCN) activity of secondary organic aerosol (SOA) and oxidized primary organic aerosol (OPOA), Atmos. Chem. Phys., 11, 8913–8928, https://doi.org/10.5194/acp-11-8913-2011, 2011.

Lee-Taylor, J., Madronich, S., Aumont, B., Baker, A., Camredon, M., Hodzic, A., Tyndall, G. S., Apel, E., and Zaveri, R. A.: Explicit modeling of organic chemistry and secondary organic aerosol partitioning for Mexico City and its outflow plume, Atmos. Chem. Phys.,
430   11, 13 219–13 241, https://doi.org/10.5194/acp-11-13219-2011, 2011.

Li, Y. and Shiraiwa, M.: Timescales of Secondary Organic Aerosols to Reach Equilibrium at Various Temperatures and Relative Humidities, Atmos. Chem. Phys., 19, 5959–5971, https://doi.org/10.5194/acp-19-5959-2019, 2019.

Li, Y., Day, D., Stark, H., Jimenez, J., and Shiraiwa, M.: Predictions of the glass transition temperature and viscosity of organic aerosols from volatility distributions, Atmos. Chem. Phys., 20, 8103–8122, https://doi.org/10.5194/acp-20-8103-2020, 2020.

435   Lim, Y. B. and Ziemann, P. J.: Effects of molecular structure on aerosol yields from OH radical-initiated reactions of linear, branched, and cyclic alkanes in the presence of NOx, Environ. Sci. Technol., 43, 2328–2334, https://doi.org/10.1021/es803389s, 2009.

Liu, X., Day, D. A., Krechmer, J. E., Brown, W., Peng, Z., Ziemann, P. J., and Jimenez, J. L.: Direct measurements of semi-volatile organic compound dynamics show near-unity mass accommodation coefficients for diverse aerosols, Commun. Chem., 2, 98, https://doi.org/10.1038/s42004-019-0200-x, 2019.

440   Mai, H., Shiraiwa, M., Flagan, R. C., and Seinfeld, J. H.: Under What Conditions Can Equilibrium Gas-Particle Partitioning Be Expected to Hold in the Atmosphere?, Environ. Sci. Technol., 49, 11 485–11 491, https://doi.org/10.1021/acs.est.5b02587, 2015.

Marshall, F. H., Berkemeier, T., Shiraiwa, M., Nandy, L., Ohm, P. B., Dutcher, C. S., and Reid, J. P.: Influence of particle viscosity on mass transfer and heterogeneous ozonolysis kinetics in aqueous-sucrose-maleic acid aerosol, Phys. Chem. Chem. Phys., 20, 15 560–15 573, https://doi.org/10.1039/c8cp01666f, 2018.

445 McVay, R. C., Zhang, X., Aumont, B., Valorso, R., Camredon, M., La, Y. S., Wennberg, P. O., and Seinfeld, J. H.: SOA formation from the photooxidation of α-pinene: Systematic exploration of the simulation of chamber data, Atmos. Chem. Phys., 16, 2785–2802, https://doi.org/10.5194/acp-16-2785-2016, 2016.

Mikhailov, E., Vlasenko, S., Martin, S. T., Koop, T., and Pöschl, U.: Amorphous and crystalline aerosol particles interacting with water vapor: Conceptual framework and experimental evidence for restructuring, phase transitions and kinetic limitations, Atmos. Chem. Phys.,

450 9, 9491–9522, https://doi.org/10.5194/acp-9-9491-2009, 2009.

Nannoolal, Y., Rarey, J., and Ramjugernath, D.: Estimation of pure component properties part 3. Estimation of the vapor pressure of non-electrolyte organic compounds via group contribution and group interactions, Fluid Phase Equilib., 269, 117–133, https://doi.org/10.1016/j.fluid.2008.04.020, 2008.

Nozière, B., Kalberer, M., Claeys, M., Allan, J., D'Anna, B., Decesari, S., Finessi, E., Glasius, M., Grgić, I., Hamilton, J. F., Hoffmann, T.,

455 Iinuma, Y., Jaoui, M., Kahnt, A., Kampf, C. J., Kourtchev, I., Maenhaut, W., Marsden, N., Saarikoski, S., Schnelle-Kreis, J., Surratt, J. D., Szidat, S., Szmigielski, R., and Wisthaler, A.: The Molecular Identification of Organic Compounds in the Atmosphere: State of the Art and Challenges, Chem. Rev., 115, 3919–3983, https://doi.org/10.1021/cr5003485, 2015.

Pajunoja, A., Malila, J., Hao, L., Joutsensaari, J., Lehtinen, K. E., and Virtanen, A.: Estimating the viscosity range of SOA particles based on their coalescence time, Aerosol Sci. Technol., 48, https://doi.org/10.1080/02786826.2013.870325, 2014.

460 Paulot, F., Crounse, J. D., Kjaergaard, H. G., Kürten, A., Clair, J. M., Seinfeld, J. H., and Wennberg, P. O.: Unexpected epoxide formation in the gas-phase photooxidation of isoprene, Science (80-.)., 325, 730–733, https://doi.org/10.1126/science.1172910, 2009.

Peeters, J., Vereecken, L., and Fantechi, G.: The detailed mechanism of the OH-initiated atmospheric oxidation of α-pinene: A theoretical study, Phys. Chem. Chem. Phys., 3, 5489–5504, https://doi.org/10.1039/b106555f, 2001.

Petters, M. D. and Kreidenweis, S. M.: A single parameter representation of hygroscopic growth and cloud condensation nucleus activity-Part

465 3: Including surfactant partitioning, Atmos. Chem. Phys., 13, 1081–1091, https://doi.org/www.atmos-chem-phys.net/7/1961/2007/, 2013.

Petters, S. S., Kreidenweis, S. M., Grieshop, A. P., Ziemann, P. J., and Petters, M. D.: Temperature- and Humidity-Dependent Phase States of Secondary Organic Aerosols, Geophys. Res. Lett., 46, 1005–1013, https://doi.org/10.1029/2018GL080563, 2019.

Pöschl, U. and Shiraiwa, M.: Multiphase Chemistry at the Atmosphere-Biosphere Interface Influencing Climate and Public Health in the Anthropocene, Chem. Rev., 115, 4440–4475, https://doi.org/10.1021/cr500487s, 2015.

470 Reid, J. P., Bertram, A. K., Topping, D. O., Laskin, A., Martin, S. T., Petters, M. D., Pope, F. D., and Rovelli, G.: The viscosity of atmospherically relevant organic particles, Nat. Commun., 9, 956, https://doi.org/10.1038/s41467-018-03027-z, 2018.

Renbaum-Wolff, L., Grayson, J. W., Bateman, A. P., Kuwata, M., Sellier, M., Murray, B. J., Shilling, J. E., Martin, S. T., and Bertram, A. K.: Viscosity of α-pinene secondary organic material and implications for particle growth and reactivity, Proc. Natl. Acad. Sci. U. S. A., 110, 8014–8019, https://doi.org/10.1073/pnas.1219548110, 2013.

475 Richards, D. S., Trobaugh, K. L., Hajek-Herrera, J., Price, C. L., Sheldon, C. S., Davies, J. F., and Davis, R. D.: Ion-molecule interactions enable unexpected phase transitions in organic-inorganic aerosol, Sci. Adv., 6, eabb5643, https://doi.org/10.1126/sciadv.abb5643, 2020.

Riva, M., Chen, Y., Zhang, Y., Lei, Z., Olson, N. E., Boyer, H. C., Narayan, S., Yee, L. D., Green, H. S., Cui, T., Zhang, Z., Baumann, K., Fort, M., Edgerton, E., Budisulistiorini, S. H., Rose, C. A., Ribeiro, I. O., Oliveira, R. L., Dos Santos, E. O., Machado, C. M., Szopa, S., Zhao, Y., Alves, E. G., De Sá, S. S., Hu, W., Knipping, E. M., Shaw, S. L., Duvoisin Junior, S., De Souza, R. A., Palm, B. B.,

480 Jimenez, J. L., Glasius, M., Goldstein, A. H., Pye, H. O., Gold, A., Turpin, B. J., Vizuete, W., Martin, S. T., Thornton, J. A., Dutcher, C. S., Ault, A. P., and Surratt, J. D.: Increasing Isoprene Epoxydiol-to-Inorganic Sulfate Aerosol Ratio Results in Extensive Conversion of

Inorganic Sulfate to Organosulfur Forms: Implications for Aerosol Physicochemical Properties, Environ. Sci. Technol., 53, 8682–8694, https://doi.org/10.1021/acs.est.9b01019, 2019.

Rothfuss, N. E. and Petters, M. D.: Influence of Functional Groups on the Viscosity of Organic Aerosol, Environ. Sci. Technol., 51, 271–279, https://doi.org/10.1021/acs.est.6b04478, 2017.

Schum, S. K., Zhang, B., Dzepina, K., Fialho, P., Mazzoleni, C., and Mazzoleni, L. R.: Molecular and physical characteristics of aerosol at a remote free troposphere site: Implications for atmospheric aging, Atmos. Chem. Phys., 18, 14 017–14 036, https://doi.org/10.5194/acp-18-14017-2018, 2018.

Seinfeld, J. H. and Pandis, S. N.: Atmospheric Chemistry and Physics: From Air Pollution to Climate Change, John Wiley, third edit edn., 2016.

Shiraiwa, M. and Pöschl, U.: Mass Accommodation and Gas-Particle Partitioning in Secondary Organic Aerosols: Dependence on Diffusivity, Volatility, Particle-phase Reactions, and Penetration Depth, Atmos. Chem. Phys., In press, https://doi.org/10.5194/acp-2020-536, 2021.

Shiraiwa, M., Ammann, M., Koop, T., and Pöschl, U.: Gas uptake and chemical aging of semisolid organic aerosol particles, Proc. Natl. Acad. Sci. U. S. A., 108, 11 003–11 008, https://doi.org/10.1073/pnas.1103045108, 2011.

Shiraiwa, M., Pfrang, C., Koop, T., and Pöschl, U.: Kinetic multi-layer model of gas-particle interactions in aerosols and clouds (KM-GAP): Linking condensation, evaporation and chemical reactions of organics, oxidants and water, Atmos. Chem. Phys., 12, 2777–2794, https://doi.org/10.5194/acp-12-2777-2012, 2012.

Shiraiwa, M., Yee, L. D., Schilling, K. A., Loza, C. L., Craven, J. S., Zuend, A., Ziemann, P. J., and Seinfeld, J. H.: Size distribution dynamics reveal particle-phase chemistry in organic aerosol formation, Proc. Natl. Acad. Sci. U. S. A., 110, 11 746–11 750, https://doi.org/10.1073/pnas.1307501110, 2013.

Shiraiwa, M., Li, Y., Tsimpidi, A. P., Karydis, V. A., Berkemeier, T., Pandis, S. N., Lelieveld, J., Koop, T., and Pöschl, U.: Global distribution of particle phase state in atmospheric secondary organic aerosols, Nat. Commun., 8, 15 002, https://doi.org/10.1038/ncomms15002, 2017.

Shrivastava, M., Cappa, C. D., Fan, J., Goldstein, A. H., Guenther, A. B., Jimenez, J. L., Kuang, C., Laskin, A., Martin, S. T., Ng, N. L., Petaja, T., Pierce, J. R., Rasch, P. J., Roldin, P., Seinfeld, J. H., Shilling, J., Smith, J. N., Thornton, J. A., Volkamer, R., Wang, J., Worsnop, D. R., Zaveri, R. A., Zelenyuk, A., and Zhang, Q.: Recent advances in understanding secondary organic aerosol: Implications for global climate forcing, Rev. Geophys., 55, 509–559, https://doi.org/10.1002/2016RG000540, 2017.

Slade, J. H., Shiraiwa, M., Arangio, A., Su, H., Pöschl, U., Wang, J., and Knopf, D. A.: Cloud droplet activation through oxidation of organic aerosol influenced by temperature and particle phase state, Geophys. Res. Lett., 44, 1583–1591, https://doi.org/10.1002/2016GL072424, 2017.

Slade, J. H., Ault, A. P., Bui, A. T., Ditto, J. C., Lei, Z., Bondy, A. L., Olson, N. E., Cook, R. D., Desrochers, S. J., Harvey, R. M., Erickson, M. H., Wallace, H. W., Alvarez, S. L., Flynn, J. H., Boor, B. E., Petrucci, G. A., Gentner, D. R., Griffin, R. J., and Shepson, P. B.: Bouncier Particles at Night: Biogenic Secondary Organic Aerosol Chemistry and Sulfate Drive Diel Variations in the Aerosol Phase in a Mixed Forest, Environ. Sci. Technol., 53, 4977–4987, https://doi.org/10.1021/acs.est.8b07319, 2019.

Song, M., Liu, P. F., Hanna, S. J., Li, Y. J., Martin, S. T., and Bertram, A. K.: Relative humidity-dependent viscosities of isoprene-derived secondary organic material and atmospheric implications for isoprene-dominant forests, Atmos. Chem. Phys., 15, 5145–5159, https://doi.org/10.5194/acp-15-5145-2015, 2015.

Song, M., Liu, P. F., Hanna, S. J., Zaveri, R. A., Potter, K., You, Y., Martin, S. T., and Bertram, A. K.: Relative humidity-dependent viscosity of secondary organic material from toluene photo-oxidation and possible implications for organic particulate matter over megacities, Atmos. Chem. Phys., 16, 8817–8830, https://doi.org/10.5194/acp-16-8817-2016, 2016.

520   Song, M., MacLean, A. M., Huang, Y., Smith, N. R., Blair, S. L., Laskin, J., Laskin, A., DeRieux, W. S. W., Li, Y., Shiraiwa, M., Nizkorodov, S. A., and Bertram, A. K.: Liquid-liquid phase separation and viscosity within secondary organic aerosol generated from diesel fuel vapors, Atmos. Chem. Phys., 19, 12 515–12 529, https://doi.org/10.5194/acp-19-12515-2019, 2019.

Tröstl, J., Chuang, W. K., Gordon, H., Heinritzi, M., Yan, C., Molteni, U., Ahlm, L., Frege, C., Bianchi, F., Wagner, R., Simon, M., Lehtipalo, K., Williamson, C., Craven, J. S., Duplissy, J., Adamov, A., Almeida, J., Bernhammer, A. K., Breitenlechner, M., Brilke, S., Dias, A.,

525   Ehrhart, S., Flagan, R. C., Franchin, A., Fuchs, C., Guida, R., Gysel, M., Hansel, A., Hoyle, C. R., Jokinen, T., Junninen, H., Kangasluoma, J., Keskinen, H., Kim, J., Krapf, M., Kürten, A., Laaksonen, A., Lawler, M., Leiminger, M., Mathot, S., Möhler, O., Nieminen, T., Onnela, A., Petäjä, T., Piel, F. M., Miettinen, P., Rissanen, M. P., Rondo, L., Sarnela, N., Schobesberger, S., Sengupta, K., Sipilä, M., Smith, J. N., Steiner, G., Tomè, A., Virtanen, A., Wagner, A. C., Weingartner, E., Wimmer, D., Winkler, P. M., Ye, P., Carslaw, K. S., Curtius, J., Dommen, J., Kirkby, J., Kulmala, M., Riipinen, I., Worsnop, D. R., Donahue, N. M., and Baltensperger, U.: The role of low-volatility

530   organic compounds in initial particle growth in the atmosphere, Nature, 533, 527–531, https://doi.org/10.1038/nature18271, 2016.

Tsigaridis, K., Daskalakis, N., Kanakidou, M., Adams, P. J., Artaxo, P., Bahadur, R., Balkanski, Y., Bauer, S. E., Bellouin, N., Benedetti, A., Bergman, T., Berntsen, T. K., Beukes, J. P., Bian, H., Carslaw, K. S., Chin, M., Curci, G., Diehl, T., Easter, R. C., Ghan, S. J., Gong, S. L., Hodzic, A., Hoyle, C. R., Iversen, T., Jathar, S., Jimenez, J. L., Kaiser, J. W., Kirkevåg, A., Koch, D., Kokkola, H., H Lee, Y., Lin, G., Liu, X., Luo, G., Ma, X., Mann, G. W., Mihalopoulos, N., Morcrette, J. J., Müller, J. F., Myhre, G., Myriokefalitakis, S., Ng, N. L., O'donnell,

535   D., Penner, J. E., Pozzoli, L., Pringle, K. J., Russell, L. M., Schulz, M., Sciare, J., Seland, Shindell, D. T., Sillman, S., Skeie, R. B., Spracklen, D., Stavrakou, T., Steenrod, S. D., Takemura, T., Tiitta, P., Tilmes, S., Tost, H., Van Noije, T., Van Zyl, P. G., Von Salzen, K., Yu, F., Wang, Z., Wang, Z., Zaveri, R. A., Zhang, H., Zhang, K., Zhang, Q., and Zhang, X.: The AeroCom evaluation and intercomparison of organic aerosol in global models, Atmos. Chem. Phys., 14, 10 845–10 895, https://doi.org/10.5194/acp-14-10845-2014, 2014.

Vaden, T. D., Imre, D., Beránek, J., Shrivastava, M., and Zelenyuk, A.: Evaporation kinetics and phase of laboratory and ambient secondary

540   organic aerosol, Proc. Natl. Acad. Sci. U. S. A., 108, 2190–2195, https://doi.org/10.1073/pnas.1013391108, 2011.

Valorso, R., Aumont, B., Camredon, M., Raventos-Duran, T., Mouchel-Vallon, C., Ng, N. L., Seinfeld, J. H., Lee-Taylor, J., and Madronich, S.: Explicit modelling of SOA formation from α-pinene photooxidation: Sensitivity to vapour pressure estimation, Atmos. Chem. Phys., 11, 6895–6910, https://doi.org/10.5194/acp-11-6895-2011, 2011.

Vereecken, L. and Peeters, J.: Decomposition of substituted alkoxy radicals - Part I: A generalized structure-activity relationship for reaction

545   barrier heights, Phys. Chem. Chem. Phys., 11, 9062–9074, https://doi.org/10.1039/b909712k, 2009.

Vereecken, L., Müller, J. F., and Peeters, J.: Low-volatility poly-oxygenates in the OH-initiated atmospheric oxidation of α-pinene: Impact of non-traditional peroxyl radical chemistry, Phys. Chem. Chem. Phys., 9, 5241–5248, https://doi.org/10.1039/b708023a, 2007.

Verwer, J. G.: Gauss–Seidel Iteration for Stiff ODES from Chemical Kinetics, SIAM J. Sci. Comput., 15, 1243–1250, https://doi.org/10.1137/0915076, 1994.

550   Verwer, J. G., Blom, J. G., and Hundsdorfer, W.: An implicit-explicit approach for atmospheric transport-chemistry problems, Appl. Numer. Math., 20, 191–209, https://doi.org/10.1016/0168-9274(95)00126-3, 1996.

Virtanen, A., Joutsensaari, J., Koop, T., Kannosto, J., Yli-Pirilä, P., Leskinen, J., Mäkelä, J. M., Holopainen, J. K., Pöschl, U., Kulmala, M., Worsnop, D. R., and Laaksonen, A.: An amorphous solid state of biogenic secondary organic aerosol particles, Nature, 467, 824–827, https://doi.org/10.1038/nature09455, 2010.

555   Virtanen, A., Kannosto, J., Kuuluvainen, H., Arffman, A., Joutsensaari, J., Saukko, E., Hao, L., Yli-Pirilä, P., Tiitta, P., Holopainen, J. K., Keskinen, J., Worsnop, D. R., Smith, J. N., and Laaksonen, A.: Bounce behavior of freshly nucleated biogenic secondary organic aerosol particles, Atmos. Chem. Phys., 11, 8759–8766, https://doi.org/10.5194/acp-11-8759-2011, 2011.

Wennberg, P. O., Bates, K. H., Crounse, J. D., Dodson, L. G., McVay, R. C., Mertens, L. A., Nguyen, T. B., Praske, E., Schwantes, R. H., Smarte, M. D., St Clair, J. M., Teng, A. P., Zhang, X., and Seinfeld, J. H.: Gas-Phase Reactions of Isoprene and Its Major Oxidation

560   Products, Chem. Rev., 118, 3337–3390, https://doi.org/10.1021/acs.chemrev.7b00439, 2018.

Ye, Q., Robinson, E. S., Ding, X., Ye, P., Sullivan, R. C., and Donahue, N. M.: Mixing of secondary organic aerosols versus relative humidity, Proc. Natl. Acad. Sci. U. S. A., 113, 12 649–12 654, https://doi.org/10.1073/pnas.1604536113, 2016.

Ye, Q., Upshur, M. A., Robinson, E. S., Geiger, F. M., Sullivan, R. C., Thomson, R. J., and Donahue, N. M.: Following Particle-Particle Mixing in Atmospheric Secondary Organic Aerosols by Using Isotopically Labeled Terpenes, Chem, 4, 318–333,

565   https://doi.org/10.1016/j.chempr.2017.12.008, 2018.

You, Y., Smith, M. L., Song, M., Martin, S. T., and Bertram, A. K.: Liquid-liquid phase separation in atmospherically relevant particles consisting of organic species and inorganic salts, Int. Rev. Phys. Chem., 33, 43–77, https://doi.org/10.1080/0144235X.2014.890786, 2014.

Zaveri, R. A., Easter, R. C., Shilling, J. E., and Seinfeld, J. H.: Modeling kinetic partitioning of secondary organic aerosol and size distribution dynamics: Representing effects of volatility, phase state, and particle-phase reaction, Atmos. Chem. Phys., 14, 5153–5181,

570   https://doi.org/10.5194/acp-14-5153-2014, 2014.

Zaveri, R. A., Shilling, J. E., Zelenyuk, A., Liu, J., Bell, D. M., D'Ambro, E. L., Gaston, C. J., Thornton, J. A., Laskin, A., Lin, P., Wilson, J., Easter, R. C., Wang, J., Bertram, A. K., Martin, S. T., Seinfeld, J. H., and Worsnop, D. R.: Growth Kinetics and Size Distribution Dynamics of Viscous Secondary Organic Aerosol, Environ. Sci. Technol., 52, 1191–1199, https://doi.org/10.1021/acs.est.7b04623, 2018.

Zaveri, R. A., Shilling, J. E., Zelenyuk, A., Zawadowicz, M. A., Suski, K., China, S., Bell, D. M., Veghte, D., and Laskin, A.: Particle-Phase

575   Diffusion Modulates Partitioning of Semivolatile Organic Compounds to Aged Secondary Organic Aerosol, Environ. Sci. Technol., 54, 2595–2605, https://doi.org/10.1021/acs.est.9b05514, 2020.

Zhang, Y., Sanchez, M. S., Douet, C., Wang, Y., Bateman, A. P., Gong, Z., Kuwata, M., Renbaum-Wolff, L., Sato, B. B., Liu, P. F., Bertram, A. K., Geiger, F. M., and Martin, S. T.: Changing shapes and implied viscosities of suspended submicron particles, Atmos. Chem. Phys., 15, 7819–7829, https://doi.org/10.5194/acp-15-7819-2015, 2015.

580   Zhang, Y., Chen, Y., Lambe, A. T., Olson, N. E., Lei, Z., Craig, R. L., Zhang, Z., Gold, A., Onasch, T. B., Jayne, J. T., Worsnop, D. R., Gaston, C. J., Thornton, J. A., Vizuete, W., Ault, A. P., and Surratt, J. D.: Effect of the Aerosol-Phase State on Secondary Organic Aerosol Formation from the Reactive Uptake of Isoprene-Derived Epoxydiols (IEPOX), Environ. Sci. Technol. Lett., 5, 167–174, https://doi.org/10.1021/acs.estlett.8b00044, 2018.

Zhang, Y., Nichman, L., Spencer, P., Jung, J. I., Lee, A., Heffernan, B. K., Gold, A., Zhang, Z., Chen, Y., Canagaratna, M. R., Jayne,

585   J. T., Worsnop, D. R., Onasch, T. B., Surratt, J. D., Chandler, D., Davidovits, P., and Kolb, C. E.: The Cooling Rate- And Volatility-Dependent Glass-Forming Properties of Organic Aerosols Measured by Broadband Dielectric Spectroscopy, Environ. Sci. Technol., 53, 12 366–12 378, https://doi.org/10.1021/acs.est.9b03317, 2019.

Zhou, S., Hwang, B. C., Lakey, P. S., Zuend, A., Abbatt, J. P., and Shiraiwa, M.: Multiphase reactivity of polycyclic aromatic hydrocarbons is driven by phase separation and diffusion limitations, Proc. Natl. Acad. Sci. U. S. A., 116, 11 658–11 663,

590   https://doi.org/10.1073/pnas.1902517116, 2019.

Ziemann, P. J. and Atkinson, R.: Kinetics, products, and mechanisms of secondary organic aerosol formation, Chem. Soc. Rev., 41, 6582–6605, https://doi.org/10.1039/c2cs35122f, 2012.

Zobrist, B., Marcolli, C., Pedernera, D. A., and Koop, T.: Do atmospheric aerosols form glasses?, Atmos. Chem. Phys., 8, 5221–5244, https://doi.org/10.5194/acp-8-5221-2008, 2008.

595   Zuend, A. and Seinfeld, J. H.: Modeling the gas-particle partitioning of secondary organic aerosol: The importance of liquid-liquid phase separation, Atmos. Chem. Phys., 12, 3857–3882, https://doi.org/10.5194/acp-12-3857-2012, 2012.